



# Characterization of a pulsed, supersonic gas jet by absorption of high-order harmonics in the extreme ultraviolet spectral range

Bastian Hagmeister<sup>1</sup> · Dirk Hemmers<sup>1</sup> · Georg Pretzler<sup>1</sup>

Received: 11 January 2022 / Accepted: 2 August 2022 / Published online: 19 August 2022  
© The Author(s) 2022

## Abstract

We present a method for determining the temporal and spatial evolution of a gas jet generated by a pulsed nozzle using high-order harmonics of a titanium–sapphire laser. This radiation in the extreme ultraviolet spectral range (17–40 nm) is transmitted through the gas jet and becomes partially absorbed depending on its wavelength and the gas density. If the absorption in this spectral range shows a sufficiently strong dependence on the wavelength, as is the case for many gases including the noble gases argon, neon, and helium, it is possible to select a proper harmonic exhibiting an absorption strong enough to generate a detectable decrease of the transmitted light but still weak enough to allow a significant amount of radiation to be transmitted through the gas jet. In the case of radial symmetry the density profile can be reconstructed by means of the Abel inversion. We show that this method allows for the determination of argon neutral densities as low as  $10^{17} \text{ cm}^{-3}$  and is also suited for other gases, such as neon and helium.

## 1 Introduction

Pulsed gas jets play an important role as targets in many fields of laser–matter interaction experiments, e.g., laser wake field acceleration, bubble acceleration of electrons, or high-harmonics generation, to name only a few. In most cases, precise knowledge and even control of the neutral gas density profile above the orifice is crucial, and therefore, its accurate measurement is of high interest. Usually, in the case of high densities, interferometric techniques are employed but their accuracy and detection limits are given by the minimal detectable fringe shift so that it is challenging to measure densities below  $10^{18} \text{ cm}^{-3}$  [1–4]. Another possibility to exploit the change of the refractive index by the probe gas is the detection of the wavefront distortion of a plane wave after being transmitted through the jet as was demonstrated in [5–7]. Further methods use ionization techniques, such as multiphoton ionization [8], strong-field ionization [9], the analysis of the plasma fluorescence during a high-harmonic generation experiment [10], or laser-induced fluorescence [11]. A last group of experiments relies on the absorption of XUV [12] or X-ray radiation [13] both making

use of monochromatic radiation, which limits the applicability to gases showing an appropriate absorption at the applied wavelength.

In this work, we propose to use high harmonics of a titanium–sapphire laser as the light source for absorption experiments. Our experiments were conducted in the spectral range between 17 and 40 nm, where the absorption coefficient of our probe gases argon, neon, and helium considerably varies with wavelength [14]. This is a great advantage over the use of only a single wavelength, because the absorption can be tuned by selecting a proper harmonic such that the gas is neither completely opaque nor nearly completely transmissive, which both would make a meaningful density determination impossible. Therefore, the use of a broad spectral range offers the option to considerably increase the range of accessible densities and allows the application to a variety of gases.

Usually, gas jets used for laser–plasma interaction experiments are expected to meet two basically contradictory requirements. First, to ensure that the interaction takes place in a confined volume with a defined density, steep gradients and a flat top density profile are required. Second, to provide enough target atoms for the interaction, high densities (preferably larger than atmospheric density) are demanded. The former can be achieved using a Laval nozzle producing a supersonic gas jet [15]. In a Laval nozzle the gas flow is continuously expanded by means of an increasing cross

✉ Dirk Hemmers  
dirk.hemmers@hhu.de

<sup>1</sup> Institut für Laser- und Plasmaphysik, Heinrich-Heine-Universität Düsseldorf, 40204 Düsseldorf, Germany

section after the minimal, i.e. critical cross section, which leads to velocities well larger than the local speed of sound. Assuming a one-dimensional, isentropic flow of an ideal gas in a nozzle with a slowly varying cross section, the pressure  $p$  along the nozzle is a function of the Mach number  $M$  and backing pressure  $p_0$  and can be expressed by

$$p = p_0 \left( 1 + \frac{\kappa - 1}{2} M^2 \right)^{\kappa/(1-\kappa)}. \quad (1)$$

In this equation  $\kappa$  denotes the adiabatic index, which amounts to 1.67 for noble gases. If the nozzle is operated at its design point, i.e. the pressure at the orifice according to Eq. (1) is equal to the ambient pressure, the gas jet propagates without a further change of its cross section, therefore, coming close to the above mentioned goals. However, if the gas jet is streaming into high vacuum as it is usually the case for laser–plasma experiments, the jet keeps expanding after leaving the orifice hence leading to a reduced density and less steep gradients. Furthermore, the gas jet may develop a pattern of standing shock waves (so-called shock diamonds), which let the jet periodically expand and re-compress so that the conditions for interaction experiments are less well-defined. To reduce this effect, high Mach numbers are required so that the pressure at the orifice converges to the ambient high vacuum. However, this results in a reduced density  $n$  at the nozzle exit, which is given by

$$n = n_0 \left( 1 + \frac{\kappa - 1}{2} M^2 \right)^{1/(1-\kappa)} \quad (2)$$

and decreases for an increasing Mach number. The concrete design of the nozzle usually is a compromise between these two requirements and demands for an accurate measurement of the spatial density distribution in front of the nozzle during the design process.

## 2 Experimental setup

The setup of our experiment is depicted in Fig. 1a. XUV radiation is generated by focussing the beam of a titanium–sapphire laser (pulse energy: 200  $\mu\text{J}$ , pulse duration: 10 fs, single shots with a repetition rate of 1 Hz) by an 800 mm parabolic mirror into an argon gas jet generated by the source nozzle. The strongly non-linear interaction taking place at an intensity of about  $1.5 \cdot 10^{14} \text{ Wcm}^{-2}$  leads to the emission of odd-numbered harmonics of the driving laser frequency roughly between H45 (17 nm) and H17 (47 nm). The radiation is filtered by two aluminum foils each having a thickness of 200 nm to remove the remaining laser light. Since the divergence of the harmonic beam is too small to allow for a complete illumination of our probe gas jet, we inserted a horizontal slit (width 20  $\mu\text{m}$ ) as a spatial filter

to diffract the beam to a width of approximately 1.5 mm FWHM at the position of the probe nozzle.

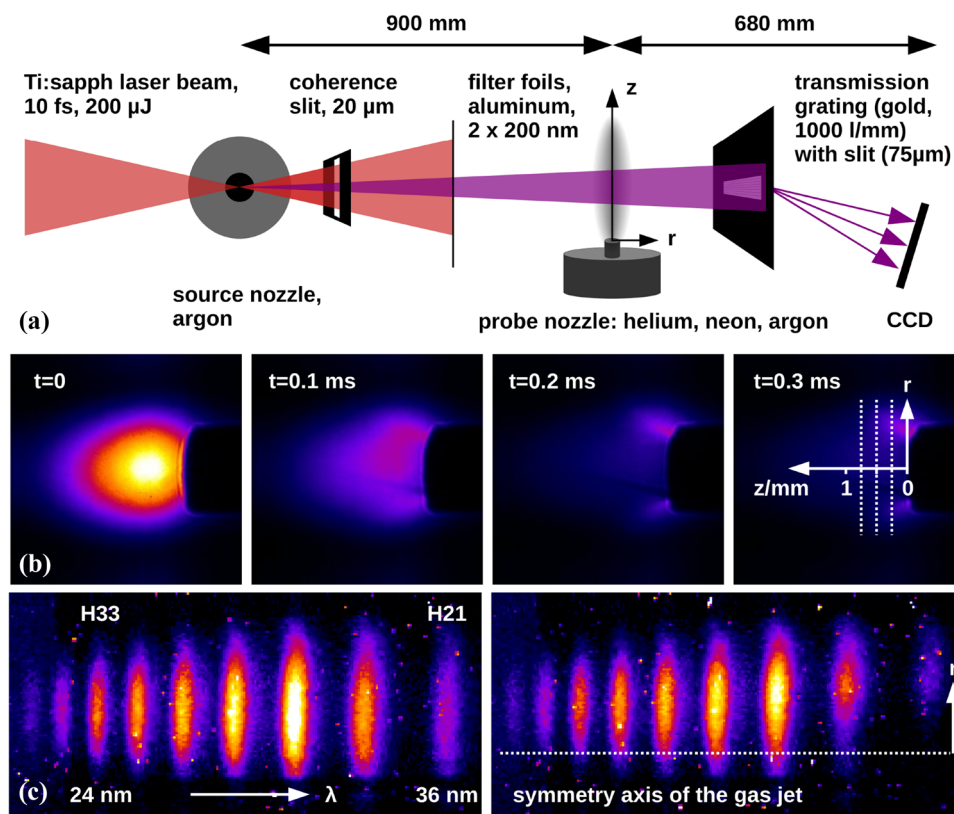
The probe nozzle is placed at a distance of 900 mm from the XUV source and is mounted on translation stages so that it can be adjusted relative to the harmonics beam and the spectrometer entrance slit. The nozzle has an inner diameter of 1.0 mm and is operated with helium, neon, or argon at a backing pressure between  $0.5 \cdot 10^5$  and  $20 \cdot 10^5$  Pa. We employed a Laval nozzle with a conically expanding cross section the design of which was developed in [3]. Our nozzle was designed and characterized in [4] by interferometric methods to achieve a Mach number of  $M = 5.5$ . Both nozzles, source and probe, are operated at the laser repetition rate of 1 Hz (limited by the pumping speed) and are triggered with respect to the pump laser of the amplifier of the titanium–sapphire laser. This allows us to conduct temporally resolved measurements with a resolution of 0.1 ms by means of applying a varying delay to the probe nozzle.

Figure 1b shows the beam geometry relative to the position of the probe nozzle (black shadow on the right hand side of each image) for different instants of the gas jet evolution. The dotted white lines indicate the  $z$ -positions, where we recorded data to obtain spatially resolved densities profiles. These positions were located 0.25 mm, 0.5 mm and 0.75 mm in front of the orifice and adjusted by moving the nozzle with respect to the spectrometer slit.

After transmission through the gas jet, the light is spectrally analyzed by a transmission grating spectrometer consisting of a gold grating with 1000 free-standing gold bars per millimetre and a 75  $\mu\text{m}$  wide slit aligned perpendicularly to the probe gas jet. As the detector, we used an Andor iKon-L CCD camera. Typical spectra are shown in Fig. 1c and extend from H21 (about 36 nm) to H35 (about 22 nm). The spectrometer is spectrally calibrated by recording the L-edge of the aluminum filters at 17 nm using harmonics generated in neon (extending to lower wavelengths but with strongly reduced efficiency). Together with the zeroth order of the grating this allows for wavelength accuracy of better than 1 %.

## 3 Experimental procedure and evaluation

Since we had to employ a small 20  $\mu\text{m}$ -slit as a spatial filter, the XUV energy flux on the camera is rather low especially after absorption by the gas jet. To obtain a sufficient signal-to-noise ratio, the CCD camera (pixel size 13.5  $\mu\text{m}$ ) was usually operated in the 4x4-binning mode and an exposure time of 720 s had to be used. For each experimental condition, a signal image and a reference image (without gas) had to be recorded to determine the line-of-sight integrated transmission. Since changes of our harmonics source during this period could not be excluded, recording of the



**Fig. 1** **a** Scheme of the experimental setup. High harmonics are generated by focussing a titanium–sapphire laser beam into an argon gas jet generated by the source nozzle. The laser beam is blocked by two aluminum filters. The harmonics beam is spatially filtered by a  $20\ \mu\text{m}$  wide slit and then transmitted through the gas jet of the probe nozzle. Hereafter, the radiation is spectrally analyzed by a transmission grating spectrometer and recorded by a CCD camera. **b** Beam geometry relative to the probe nozzle (black shadows) for different instants

of the gas jet evolution. The white dotted lines indicate the different positions in front of the nozzle, where we recorded density profiles. **c** Typical harmonic spectra (left image: without probe gas jet, right image: with argon probe gas jet with a backing pressure of  $1 \cdot 10^5\ \text{Pa}$ ). The dashed line indicates the axis of the gas jet. Notice that the nozzle has been shifted with respect to the images in **b**) to detect the boundary of the gas jet

signal and reference image was alternated after each 120 s to account for a possible drift. The resulting 6 images were combined to the final image so that for each image harmonics were accumulated over 720 laser pulses.

Figure 1b shows the temporal evolution of the total absorption within 0.3 ms after the probe nozzle was opened. The gas density increases with advancing time and the absorption of the harmonic radiation becomes stronger. The shadow of the gas jet is found in good approximation to be identical on either side of the  $z$ -axis indicating rotational symmetry, which is a prerequisite for further analysis by the Abel inversion. Due to geometrical restrictions we used only one half of the image for evaluation.

Figure 1c shows two typical spectra, which serve as a reference image (left hand side) and a signal image (right hand side) for an argon probe jet with a backing pressure of  $1 \cdot 10^5\ \text{Pa}$ . These spectra were recorded 0.5 mm in front of the orifice of the nozzle. The axis of the gas jet is indicated by the horizontal dashed line. Argon exhibits a strong

decrease of transmission between 25 nm and 30 nm so that the gas is nearly opaque for H21 in the center of the jet and no meaningful determination of its density would be possible. However, for H23 to H27 the absorption is suitably strong so that we can determine the argon density.

The typical evaluation procedure is exemplified in Fig. 2. Assuming radial symmetry of the absorption coefficient  $\alpha(r)$ , the lateral intensity distribution  $I(y)$  measured behind the gas jet can be calculated from the incoming intensity  $I_0(y)$  by

$$\ln \frac{I_0(y)}{I(y)} = 2 \int_y^\infty \alpha(r) \frac{r \, dr}{\sqrt{r^2 - y^2}}. \quad (3)$$

This equation can in principle be solved for the absorption  $\alpha(r)$  by the well-known Abel inversion [16], which is, however, not directly applicable to the measured data, since the required first derivative of  $I_0/I$  would introduce unacceptable errors. To circumvent this problem, we used the method proposed in [17], which uses a Fourier series to model the

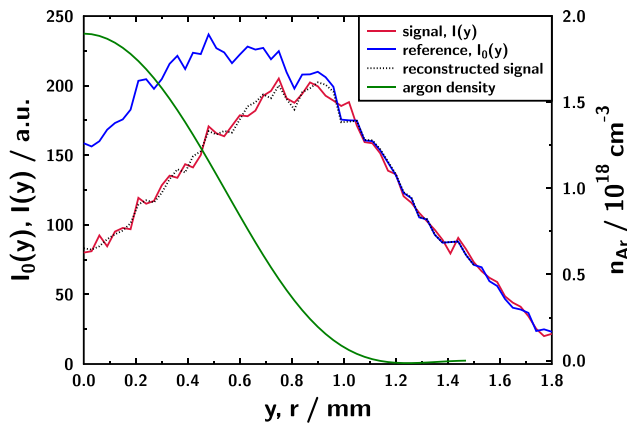


**Fig. 2** Typical lateral intensity profiles  $I_0(y)$  (reference) and  $I(y)$  (signal) for H25 for an argon gas jet with a backing pressure of  $1 \cdot 10^5$  Pa. The dashed line indicates the reconstructed intensity  $I(y)$  as determined by the left-hand side of Eq. (3) from the best fit of  $\alpha(r)$  and  $I_0(y)$ . The green curve shows the resulting argon density profile

function  $\alpha(r)$  so that the right-hand side of Eq. (3) is numerically fitted to the measured data, i.e. the left-hand side of Eq. (3). Once the absorption coefficient is known, the absorber density  $n$  is given by  $n = \alpha/\sigma$  with  $\sigma$  denoting the cross section for absorption taken from [14].

The result of this procedure is shown in Fig. 2. It is seen that the reconstructed signal fits well to the measured curve leading to a neutral density of  $1.9 \cdot 10^{18} \text{ cm}^{-3}$  in the center of the jet with a spatial profile close to a Gaussian. The full width at half maximum of the profile corresponds to the nozzle diameter. Note that this method can lead to slightly negative densities in the boundary region of the gas jet due to the use of oscillating functions in the fitting procedure. Usually it is possible to conduct this evaluation for three different harmonics. The variation of these results allows for an error estimate including the statistical error due to the shot noise and systematic errors caused by background subtraction, hot pixel correction, and a potential drift of the light source. Typically, our results vary about 10 % around the mean, which we assume to represent the accuracy of the presented data.

### 4 Results and discussion

In a first step we looked at the temporal evolution of the gas density after the valve of the nozzle was opened. The resulting curve is shown in Fig. 3. The origin of the time axis is set arbitrarily to the instant when we first could detect a significant amount of gas. We find that a steady state of the gas flow develops after a rise time of about 0.5 ms, which remains constant within our accuracy for at least 1 ms. Regarding a possible application of this nozzle in,

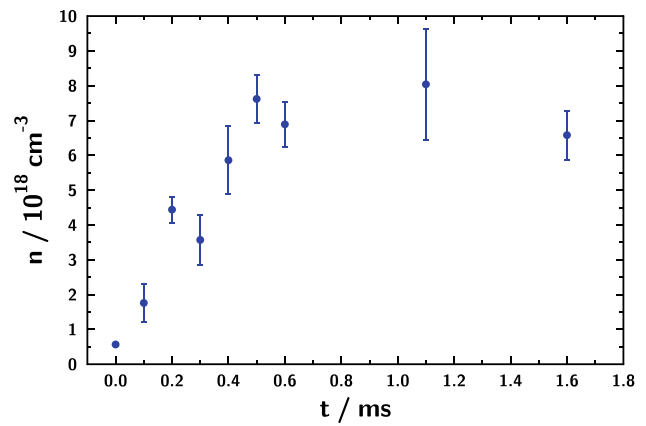


**Fig. 3** Temporal evolution of the on-axis density in a distance of  $z = 0.5$  mm from the orifice for an argon gas jet with a backing pressure of  $10 \cdot 10^5$  Pa

e.g., laser–plasma experiments, two points are worth noting. First, the achievement of a steady state is a prerequisite for reproducible experiments. Second, a fast rise time of 0.5 ms is important in order not to fill the vacuum chamber with gas before the steady state is reached and the laser is fired. All further data we show were recorded during the steady state of the gas flow.

In our second experiment we varied the argon backing pressure between  $0.5 \cdot 10^5$  Pa and  $20 \cdot 10^5$  Pa. The measured argon density profiles are shown in Fig. 4. Notice that we were able to detect on-axis densities as low as  $10^{18} \text{ cm}^{-3}$  in the case of the lowest backing pressure by means of H21 ( $\lambda = 37$  nm). Using longer wavelengths, e.g., H17 ( $\lambda = 47$  nm), and exploiting their stronger absorption, it would be possible to achieve a detection limit of a few

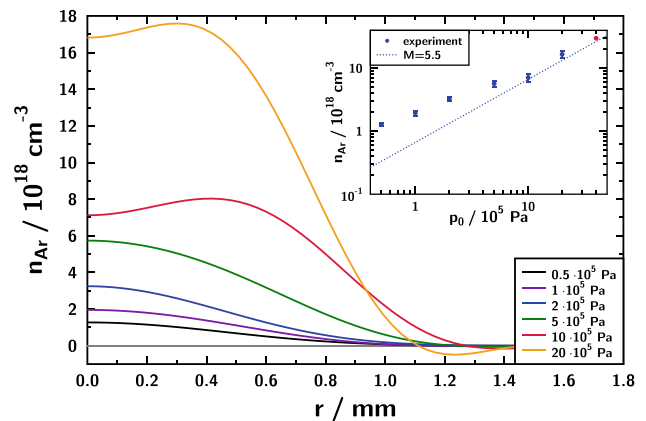


**Fig. 4** Argon density profiles for a varying backing pressure in a distance of 0.5 mm from the orifice. The inset shows the on-axis density as a function of the backing pressure. The red dot shows the result of an interferometric measurement conducted in [4]. The dashed line shows the density according to Eq. (2) for the design goal of  $M = 5.5$

$10^{17} \text{ cm}^{-3}$  for our gas jet diameter of about 1 mm. The commonly used interferometric technique on the other hand would be required to determine a fringe shift of about  $\lambda/100$  to achieve a comparable detection limit. Furthermore, our method allows for an easy detection of helium, which is similar to argon regarding its absorption length. On the other hand, its refractive index decrement is lower by one order of magnitude compared with argon thus making an interferometric detection challenging.

The measured neutral density profiles are close to a Gaussian for lower backing pressures but exhibit a nearly flat-top profile with steeper gradients for high pressures. Notice that the slight hollow profiles are likely an artifact from the Abel inversion. The on-axis densities as a function of backing pressure are shown in the inset in Fig. 4. Note that these values fit well to the density of  $3 \cdot 10^{19} \text{ cm}^{-3}$  for a backing pressure of  $40 \cdot 10^5 \text{ Pa}$  measured by an interferometric method in [4]. Comparing the experimental data with the original design goal of  $M = 5.5$  (blue dashed curve according to Eq. (2)) we find that it is almost achieved by the nozzle under consideration, especially for high backing pressures. However, at low backing pressures, densities are found to increase slightly less than proportional to  $p_0$ . A possible reason is that the employed one-dimensional model oversimplifies the situation, which is also indicated by the change of the spatial profiles from Gaussian to flat-top showing that two-dimensional effects are relevant and influence the fluid dynamics involved.

In Fig. 5 we show density profiles recorded at different distances from the orifice illustrating the expansion of the gas jet after leaving the orifice. At a distance of 0.25 mm the jet is more confined and its on-axis density is higher than at 0.5 mm distance. At the larger distance of 0.75 mm the density drops further indicating a further expansion of the gas jet as would be expected in the case the nozzle

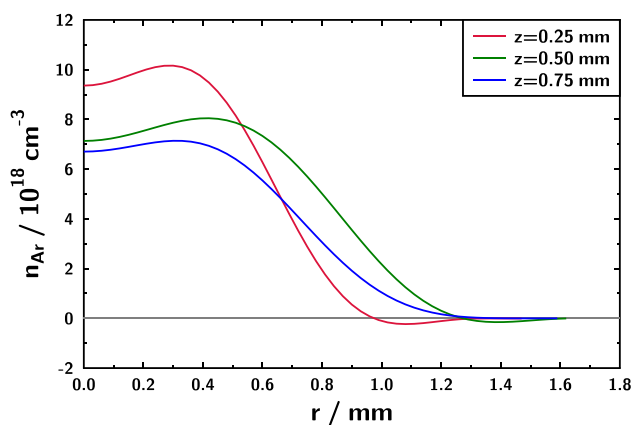


**Fig. 5** Argon density profiles for increasing distance  $z$  from the orifice for a backing pressure of  $10 \cdot 10^5 \text{ Pa}$

is not operated at its design point but at a point, where the exhaust pressure ( $p = 2.4 \cdot 10^3 \text{ Pa}$  for a nozzle with  $M = 5.5$  and a backing pressure of  $p_0 = 10 \cdot 10^5 \text{ Pa}$ ) is larger than the ambient pressure.

Finally, we would like to demonstrate that this methods works well also for other gases, especially for helium. Figure 6 shows measured density profiles for the nobles gases helium, neon, and argon for a backing pressure of  $1 \cdot 10^5 \text{ Pa}$ . According to Eq. 2 gases with equal adiabatic index  $\kappa$  behave the same. From our experiments we find that the corresponding densities profiles are equal within our accuracy. For heavier gases there seems to be a slight systematic tendency to lower densities, however, to resolve this issue, detailed numerical simulations of the fluid dynamics would be required, which is beyond the scope of this paper.

## 5 Summary and conclusions

We have shown that the absorption of high-order harmonics in the XUV spectral range is a reliable method to determine neutral density profiles in a pulsed gas jet with an accuracy of about 10 %. The selection of a proper harmonic exhibiting an appropriate absorption has the advantage that a large range of densities with a detection limit as low as several  $10^{17} \text{ cm}^{-3}$  is accessible. Thus, the method is very versatile regarding spatially and temporally resolved measurements, which might on the one hand require to detect low densities in the wings of the jet or at the beginning or close to the end of a pulse or, on the other hand, high densities close to the pulse peak. Since helium and neon have similar absorption lengths in the considered spectral range, this method is also well suited for these two gases. This is a clear benefit of our method compared with methods relying on the refractive index of the probed gas, especially in the case of helium, which is challenging to probe with, e.g., interferometric

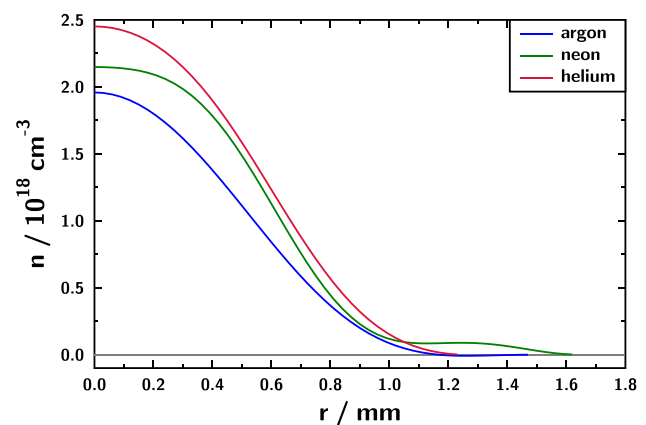


**Fig. 6** Measured density profiles of helium, neon, and argon for a backing pressure of  $1 \cdot 10^5 \text{ Pa}$



methods. Our experimental results are consistent with theoretical expectations concerning the employed probe nozzle, which was designed to produce a supersonic gas jet. This method is, therefore, useful for the design and test procedures associated with these kinds of gas targets by extending the dynamic range and the variety of accessible gases.

**Funding** Open Access funding enabled and organized by Projekt DEAL.

**Open Access** This article is licensed under a Creative Commons Attribution 4.0 International License, which permits use, sharing, adaptation, distribution and reproduction in any medium or format, as long as you give appropriate credit to the original author(s) and the source, provide a link to the Creative Commons licence, and indicate if changes were made. The images or other third party material in this article are included in the article's Creative Commons licence, unless indicated otherwise in a credit line to the material. If material is not included in the article's Creative Commons licence and your intended use is not permitted by statutory regulation or exceeds the permitted use, you will need to obtain permission directly from the copyright holder. To view a copy of this licence, visit <http://creativecommons.org/licenses/by/4.0/>.

## References

1. J. Nejd, J. Vančura, K. Boháček, M. Albrecht, U. Chaulagain, *Rev. Sci. Instr.* **90**, 065107 (2019)
2. V. Malka, C. Coulaud, J.P. Geindre, V. Lopez, Z. Najmudin, D. Neely, F. Amiranoff, *Rev. Sci. Instrum.* **71**, 2329–2333 (2000)
3. S. Semushin, V. Malka, *Rev. Sci. Instrum.* **72**, 2961 (2001)
4. R. Jung, Laser-plasma interaction with ultra-short laser pulses (Dissertation Heinrich-Heine-Universität Düsseldorf 2007) 59–72
5. C. Peth, S. Kranzusch, K. Mann, *Rev. Sci. Instrum.* **75**, 3288 (2004)
6. T. Mey, M. Rein, P. Großmann, K. Mann, *New J. Phys.* **14**, 1–15 (2012)
7. J. Holburg, M. Müller, K. Mann, *Opt. Express* **29**, 6620–6628 (2021)
8. N.E. Schofield, D.M. Paganin, A.I. Bishop, *Rev. Sci. Instrum.* **80**, 123105 (2009)
9. O. Tchulov, M. Negro, S. Stagira, M. Devetta, C. Vozzi, E. Frumker, *Sci. Rep.* **7**, 6905 (2017)
10. A. Comby, S. Beaulieu, E. Constant, D. Descamps, S. Petit, Y. Mairesse, *Opt. Express* **26**, 6001–6009 (2018)
11. B.H. Faylor, S. Chantrenne, P.L. Coleman, J.S. Levine, Y. Song, H.M. Sze, *Rev. Sci. Instrum.* **74**, 1070 (2003)
12. P.W. Wachulak, Ł. Węgrzyński, Z. Ząprażny, A. Bartnik, T. Fok, R. Jarocki, J. Kostecki, M. Szczurek, D. Korytár, H. Fiedorowicz, *Appl. Phys. B* **117**, 253–263 (2014)
13. R. Rakowski, A. Bartnik, H. Fiedorowicz, R. Jarocki, J. Kostecki, J. Mikołajczyk, A. Szczurek, M. Szczurek, I.B. Földes, Zs. Tóth, *Nucl. Instrum. Methods Phys. Res. A* **551**, 139–144 (2005)
14. G.V. Marr, J.B. West, *Atomic Data Nucl. Data Tab.* **18**, 497–508 (1976)
15. R. Fitzpatrick, *Theoretical fluid mechanics* (IoP publishing, Bristol, 2017). (**chapter 14**)
16. N.H. Abel, *J. für die reine und angew. Math.* **1**, 153–157 (1826)
17. G. Pretzler, *Z. Naturforsch.* **46a**, 639–641 (1991)

**Publisher's Note** Springer Nature remains neutral with regard to jurisdictional claims in published maps and institutional affiliations.